

Detect Changes like Humans: Incorporating Semantic Priors for Improved Change Detection

Yuhang Gan, Wenjie Xuan, Zhiming Luo, Lei Fang, Zengmao Wang, *Member, IEEE*,
Juhua Liu, *Member, IEEE*, Bo Du, *Senior Member, IEEE*

Abstract—When given two similar images, humans identify their differences by comparing the appearance (e.g., color, texture) with the help of semantics (e.g., objects, relations). However, mainstream change detection models adopt a supervised training paradigm, where the annotated binary change map is the main constraint. Thus, these methods primarily emphasize the difference-aware features between bi-temporal images and neglect the semantic understanding of the changed landscapes, which undermines the accuracy in the presence of noise and illumination variations. To this end, this paper explores incorporating semantic priors to improve the ability to detect changes. Firstly, we propose a Semantic-Aware Change Detection network, namely SA-CDNet, which transfers the common knowledge of the visual foundation models (i.e., FastSAM) to change detection. Inspired by the human visual paradigm, a novel dual-stream feature decoder is derived to distinguish changes by combining semantic-aware features and difference-aware features. Secondly, we design a single-temporal semantic pre-training strategy to enhance the semantic understanding of landscapes, which brings further increments. Specifically, we construct pseudo-change detection data from public single-temporal remote sensing segmentation datasets for large-scale pre-training, where an extra branch is also introduced for the proxy semantic segmentation task. Experimental results on five challenging benchmarks demonstrate the superiority of our method over the existing state-of-the-art methods. The code is available at [SA-CD](#).

Index Terms—Change Detection, Pre-training, Dual-stream Decoder, Semantic-aware, Multi-scale Feature

I. INTRODUCTION

REMOTE sensing change detection identifies interested landscape changes and interprets variations from bi-temporal images covering the same region [1–3]. It plays a crucial role in environmental monitoring, natural disaster assessment, urban planning, *etc.* To handle change detection

This work was supported in part by the National Natural Science Foundation of China under Grants U23B2048 and 62225113, in part by the Innovative Research Group Project of Hubei Province under Grant 2024AFA017, in part by the Science and Technology Major Project of Hubei Province under Grant 2024BAB046, in part by Major Special Project of China Innovation Challenge (Ningbo) under Grant 2024T008, and in part by the Science and Technology Project of State Grid Corporation of China under Grant 5700-202458333A-2-1-ZX. The numerical calculations in this paper have been done on the supercomputing system in the Supercomputing Center of Wuhan University. *Y. Gan and W. Xuan contributed equally to this work. Corresponding authors: Zengmao Wang, Juhua Liu (e-mail: {wangzengmao, liujuhua}@whu.edu.cn).*

Y. Gan, W. Xuan, Z. Luo, J. Liu and B. Du are with the School of Computer Science, National Engineering Research Center for Multimedia Software, and Institute of Artificial Intelligence, Wuhan University, Wuhan, China. Y. Gan is also with Land Satellite Remote Sensing Application Center, MNR, Beijing, China (e-mail: {ganyuhang, dreamxwj, thislzm, wangzengmao, liujuhua, dubo}@whu.edu.cn).

L. Fang is with CAAZ(Zhejiang) Information Technology Co., Ltd., Ningbo, China. (e-mail: icedark@zju.edu.cn).

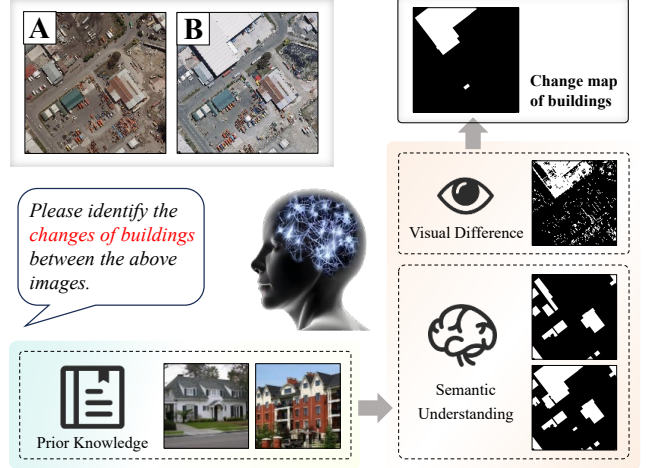


Fig. 1: To locate changes between two images, humans not only perceive appearance differences but also utilize semantic priors unconsciously for help. For instance, humans would identify subjects in each image via prior knowledge and then compare them, which reflects the importance of semantics in detecting changes. However, current change detection methods are inclined to learn difference-aware features through the target difference map for training, while ignores semantic understandings and brings sub-optimal results.

with massive high-resolution remote sensing images effectively and efficiently, deep-learning-based methods have grown prosperity for their powerful representation capability and impressive performance in recent years.

Current deep-learning-based change detection methods [4–11] mostly employed a siamese architecture with supervised training strategy, consisting of a network to extract features and a classifier to discriminate changed regions. Most methods adopted Convolutional Neural Networks (CNNs) [4, 5] or Vision Transformer (ViT) [6, 7] as the feature extractor to provide discriminative representations for bi-temporal images. The classifier usually selects a fully connected or softmax layer to backpropagate loss. The main supervision is a binary difference map that represents the interested subject changes between the bi-temporal images. Previous methods [8–10] aim to learn an informative feature space where the features of the changed pixels are pushed apart and those unchanged ones are pulled together. Since the binary difference map only provides the change information, such methods are inclined to learn difference-aware features. Therefore, *they would fall short of learning semantic-aware features, which deviates from*

the human visual paradigm and leads to sub-optimal results. As illustrated in Fig. 1, when given two images of the same area, humans find the changed regions encouraged by both the appearance difference and semantics [12]. Generally, the appearance differences represent the absolute visual changes between the two images. Such differences would be caused by multiple factors (*e.g.*, seasonal or illumination variations) apart from the true landscape changes. In contrast, the semantics are utilized unconsciously, but it is helpful and vital to distinguish the interested subject changes such as the buildings and farmland. Motivated by this observation, this paper explores incorporating semantic priors for improved performance on change detection.

This paper proposes to enhance the semantic understanding of the changed landscapes from three aspects: **i)** We employ the vision foundation model (*i.e.*, *FastSAM* [13]) to encode features and adapt it to change detection via an adapter. This design endows the network with rich knowledge stored in the foundation model, providing rich priors of natural images. **ii)** Inspired by the human visual paradigm, a dual-stream feature decoder is proposed to extract difference-aware features and semantic-aware features individually. Such features are proved to be complementary in our experiments, especially when pixel-level variations exist. Thus, we propose an advanced network for change detection, namely SA-CDNet. **iii)** To further enrich the semantic understanding of landscapes, a novel single-temporal semantic pre-training strategy is designed. We first leverage remote sensing semantic segmentation data to construct large-scale pseudo-change detection data, which are used to pre-train the whole SA-CDNet for change detection. Moreover, we further introduce an extra branch for semantic segmentation as an additional pre-training task, encouraging better understandings of the interested landscapes.

Our main contributions can be summarized as follows:

- We propose an advanced SA-CDNet for change detection, which inherits the rich knowledge of natural images from the vision foundation model and adapts these semantic priors to remote sensing change detection. Besides, a dual-stream feature decoder is derived to mimic the human visual paradigm, which consists of a semantic-aware decoder branch and a difference-aware decoder branch for robust predictions.
- A well-designed single-temporal semantic pre-training strategy is proposed to enhance the semantic understanding of landscapes further. We construct pseudo-change detection data from remote sensing semantic segmentation datasets to pre-train the network. An extra segmentation branch is also introduced for improved semantic understanding through discriminating landscapes in single-temporal images.
- Extensive experiments are conducted on five challenging benchmarks, *i.e.*, LEVIR-CD, LEVIR-CD+, S2Looking, WHU-CD for building changes, and the WHU Cultivated Land for farmland changes. Our method achieves SOTA performance on all datasets. We also ablate the modules and discuss different settings for the pre-training in detail to prove their effectiveness.

The rest of the paper is organized as follows. Sec. II gives an overview of the related works. Sec. III introduces the proposed SA-CDNet and the pre-training strategy. Sec. IV includes a series of experiments and ablation studies on five benchmarks. Finally, Sec. V concludes the paper.

II. RELATED WORK

A. Remote Sensing Change Detection

Change detection has been a long-standing challenge within the remote sensing domain. Early methods relied on intuitive pixel value comparisons to identify changes, including image algebra [14] or image transformation [15]. But these approaches were sensitive to noise and hard to find universally suitable thresholds. The advent of GIS and the availability of spatiotemporal datasets encouraged researchers to apply machine-learning techniques to change detection like decision trees [16, 17], support vector machines [18, 19], *etc.* Though these methods improved accuracy, they could not handle complicated real-life scenarios well and their performance was constrained by the manually-designed representations.

Recent improvements of change detection techniques were mainly attributed to the advanced deep-learning methods [3]. The pioneer work [20] proposed a siamese structure based on U-Net for change detection, which leveraged CNNs to capture local spatial context and yielded attractive performance. To cover the information loss during the successive down-sampling in CNNs, SNUNet [21] introduced dense skip connections and multi-scale feature fusion to enhance representations for detecting detailed changes. ViT [22] were introduced to change detection due to their global context representations. SwinSUNet [23] constructed a fully transformer-based encoder-decoder network for change detection based on Swin Transformer. Similarly, BIT [24] utilized the self-attention mechanism of transformers to capture global features, thereby enhancing change detection performance.

The above methods primarily focus on enhancing representations through advanced network architectures or attention mechanisms to realize increments. However, given that only binary difference maps are available for supervised training in change detection tasks, existing studies focused on difference-aware features and overlooked the enhancement of semantic understandings. We argue that this deviates from the human visual paradigm, where both pixel difference and semantics are crucial in distinguishing subject changes. Therefore, this paper primarily explores the incorporation of richer semantic priors into change detection for improvements.

B. Vision Foundation Models

Recently, vision foundation models [25] have raised great attention in computer vision. By training models with billions of parameters on extensive data, these models not only demonstrate promising performance but also exhibit unparalleled capability of understanding image contents and zero-shot generalization to unseen subjects. The representative SAM [26] can segment any object of interest with high accuracy through prompting. Inspired by its great success, many variants have been proposed. SEEM [27] expanded the prompt type of

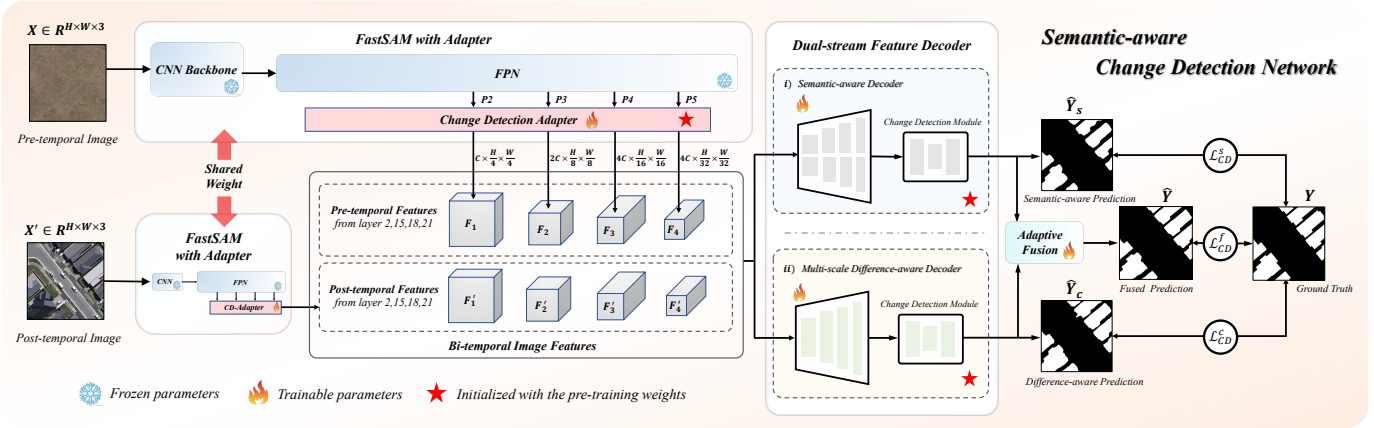


Fig. 2: The overview of SA-CDNet. We employ the frozen FastSAM encoder to extract features, then refined by an adapter to align features for change detection task. The dual-stream feature decoder contains a semantic-aware feature decoder and a multi-scale difference-aware feature decoder, providing richer semantic-aware and difference-aware features. The adaptive fusion module combines such features and produces the final change map. Note that the adapter and dual-stream decoder are initialized with the proposed single-temporal semantic pre-training strategy.

SAM to multi-modal prompts for more flexible segmentation. [13, 28, 29] accelerated SAM by replacing its encoder with lightweight alternatives, making it more efficient and easier for deployment. [30, 31] extended the application to the medical domain, achieving considerable performance. Recent studies [32–34] endeavored to marry SAM for change detection, leveraging its powerful representations and semantic understanding for advanced performance. BAN [32] froze the foundation model and introduced an additional bi-temporal adapter to transfer its inner knowledge of natural images to change detection tasks. Concurrently, SAM-CD [33] applied FastSAM to change detection with an adapter. It also introduced a task-agnostic semantic learning branch to encourage similar representations of unchanged areas. SCD-SAM [34] combined MobileSAM [29] and CNN into a contextual semantic-aware dual encoder with adapters to detect semantic changes. It employed a dual decoder to aggregate bi-temporal features, thus mitigating the semantic gap across scales.

Although our SA-CDNet shares similar ideas with SAM-CD in adapting vision foundation models to change detection, we claim that our work varies from it. Our method explores the crucial role of semantic priors in change detection. The proposed dual-stream feature decoder yields more accurate results than SAM-CD, attributed to the integration of richer semantic-aware and difference-aware representations. Furthermore, the proposed single-temporal semantic pre-training further enhances the semantic priors of landscapes.

III. METHODOLOGY

This section first reveals the detailed structure of our SA-CDNet in Sec. III-A. Sec. III-B introduces the proposed single-temporal semantic pre-training strategy, including the pseudo-change detection data construction and the proxy segmentation task design. Then, the overall “pre-training + fine-tuning” pipeline is concluded in Sec. III-C.

A. Semantic-aware Change Detection Network

The overall architecture of SA-CDNet is presented in Fig. 2, primarily consisting of three components: **i)** A vision foundation model-based feature encoder (*i.e.*, FastSAM) with a change detection adapter to provide discriminative representations. **ii)** A dual-stream feature decoder, containing a semantic-aware decoder branch and a multi-scale difference-aware branch, to decode semantic-aware and difference-aware features for human-like change detection. **iii)** An adaptive fusion module to combine the semantic-aware and difference-aware features for change predictions.

When given bi-temporal images $X, X' \in \mathbb{R}^{H \times W \times 3}$, the network would produce a binary change map $\hat{Y} = \{y_{ij} \in \{0, 1\}\}^{H \times W}$ representing the changed regions. Y denotes the ground-truth change map. Specifically, the vision foundation model-based feature encoder $\mathcal{E}(\cdot)$ first extracts features from the two images separately at the FPN [35], denoted as $\{P_i, P'_i\}_{i=2,3,4,5}$. Since the vision foundation model is commonly pre-trained on extensive natural scene image datasets, it keeps rich semantic priors of natural images. We freeze its parameters to keep its inner knowledge unaffected when adapting it to change detection. Besides, similar to SAM-CD, an adapter $\mathcal{A}(\cdot)$ is introduced to align the features to remote sensing images for change detection tasks, denoted as $\{F_i, F'_i\}_{i=2,3,4,5}$. Then, these refined features would be fed to the dual-stream decoder to further mine semantic-aware features $\{S_i, S'_i\}_{i=2,3,4,5}$ through the semantic-aware decoder branch $\mathcal{M}(\cdot)$ and difference-aware features $\{D_i, D'_i\}_{i=2,3,4,5}$ through the multi-scale difference-aware decoder branch $\mathcal{N}(\cdot)$ independently. Finally, the adaptive fusion module would complement difference-aware features with the semantic-aware features and predict the change map \hat{Y} with a softmax classifier. The ground truth Y is used to compute the loss. For a better understanding, we elaborate on the detailed structure and designs of each module as follows.

1) Vision foundation model-based feature encoder with change detection adapter: Recently, vision foundation models

like SAM [26] and its variants [13, 27–30] have shown impressive performance and zero-shot ability on semantic segmentation and displayed profound semantic understandings of the subjects in the natural images. To marry the rich semantic priors of vision foundation models for change detection, we borrow the feature encoder of vision foundation models to obtain discriminative features from bi-temporal images first. Note that we have compared SAM and its three variants, including EfficientSAM [28], FastSAM [13], and MobileSAM [29] in Sec. IV-B, and finally selected FastSAM as encoder since the trade-off between performance and efficiency. We highlight that *the FastSAM encoder can be substituted by that of another foundation model* because we only employ the frozen encoder to extract bi-temporal image features. Specifically, the FastSAM feature encoder inherits the Yolo-v8 structure, which comprises a CNN backbone with FPN to extract features. We input the bi-temporal images separately and select the features from the 2nd, 15th, 18th, and 21st layers (*i.e.*, the final layer of each stage) as $\{P_i, P'_i\}_{i=2,3,4,5}$. We freeze the parameter of the pre-trained FastSAM to avoid negative impacts on its inner knowledge.

Considering the semantic gap between natural images and remote sensing images, we follow SAM-CD and introduce an adapter $\mathcal{A}(\cdot)$ for feature alignment as shown in Fig. 2, thus adapting representations to change detection. The adapter contains a 1×1 convolution, batch normalization, and ReLU function. The process of feature alignment can be denoted as:

$$F_i = A(P_i) = \text{ReLU}\{\text{BN}[\text{Conv}(P_i)]\}, \quad (1)$$

where P_i and F_i are the selected features of FastSAM and the output aligned features, respectively. This adapter enables the features extracted from the frozen vision foundation model to fit change detection task better.

2) **Dual-stream feature decoder:** Motivated by the fact that humans rely on both the appearance difference and semantics to identify changed regions, we design a dual-stream feature decoder to mine semantic-aware features and difference-aware features separately for improved performance. The detailed structures of the two branches are revealed as follows.

Semantic-aware decoder $\mathcal{M}(\cdot)$ employs a simple network that contains three decoding units to decode bi-temporal features individually. As shown in Fig. 3(a), each decoding unit comprises an up-sampling and two conv + batch norm + ReLU blocks, progressively fusing multi-scale features of single-temporal images. Taking unit i for example, it receives decoded features D_{i+1} from the previous stage, performs deconvolution to upsample D_{i+1} , then concatenates it with the current feature F_i and feeds to the decoder unit. The extracted features $\{F_i, F'_i\}_{i=2,3,4,5}$ come from four scales ($\frac{H}{4k}, \frac{W}{4k}$) $_{k=1,2,4,8}$, which is expressed as,

$$D_i = \text{Conv}[F_i, \text{Upsample}(D_{i+1})], \quad D_4 = F_4. \quad (2)$$

Then the decoded features D_4, D'_4 are further concatenated and fed to a change detection module that consists of two convolutional blocks and a sigmoid layer for change prediction. Thus, the overall computation of the semantic-aware decoder branch is formulated as,

$$\hat{Y}_s = \mathcal{M}(\{F_i, F'_i\}_{i=2,3,4,5}), \quad (3)$$

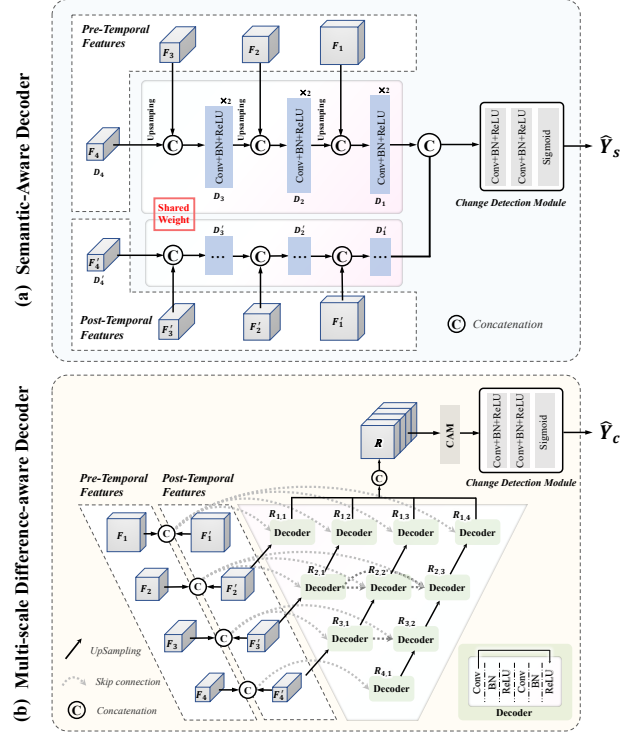


Fig. 3: The structure of dual-stream feature decoder, which includes (a) the semantic-aware decoder and (b) the multi-scale difference-aware decoder.

where \hat{Y}_s is the output semantic-aware change map. Since bi-temporal image features are extracted and fused independently, we suppose this design helps to keep the semantics of single-temporal images. Besides, the late fusion of bi-temporal image features implicitly exploits the landscape semantics to distinguish changed regions. As validated in Sec. IV-B, the semantic-aware decoder is advanced to capture subject semantics and is robust to seasonal and illumination variations.

Multi-scale difference-aware decoder $\mathcal{N}(\cdot)$ takes a densely connected structure as presented in Fig. 3(b). The basic decoding unit consists of two conv + batch norm + ReLU blocks. Given the extracted $\{F_i, F'_i\}_{i=2,3,4,5}$, the feature maps of the same scale are first concatenated and then delivered to the densely-connected decoding units, in order to mine difference-aware features. Following SNUNet [21], each unit also receives features from adjacent scales to enrich multi-scale representations. This process can be expressed as,

$$R_{i,j} = \begin{cases} \text{Conv}[F_i, F'_i, \text{Up}(F'_i)] & j = 1, \\ \text{Conv}[F_i, F'_i, [R_{i,k}]_k^{j-1}, \text{Up}(R_{i+1,j-1})] & j > 1, \end{cases} \quad (4)$$

where $R_{i,j}$ denotes the output of the (i, j) decoding unit. F_i, F'_i are pre- and post-temporal image features. Up means the upsampling with deconvolution. After the decoding process, the fused multi-scale features $\{R_{1,j}\}_{j=1,2,3,4}$ are collected. We employ a Channel Attention Module (CAM) [36] to integrate all difference information, and use a change detection module with the sigmoid function to predict the difference-aware change map \hat{Y}_c . The overall computation of multi-scale

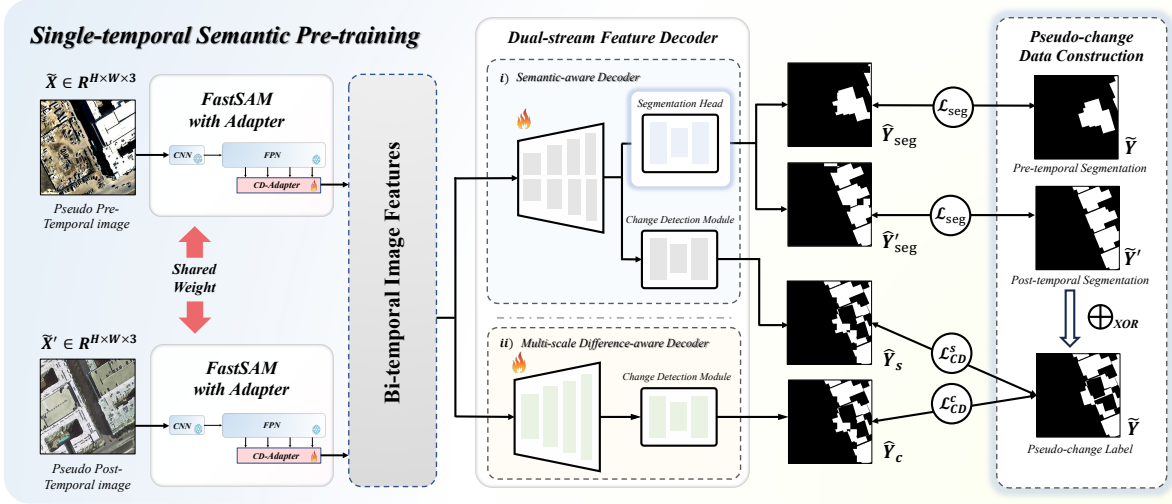


Fig. 4: The pipeline of single-temporal semantic pre-training. We first construct pseudo-change data from the single-temporal semantic segmentation datasets, providing a large-scale dataset with full annotations for pre-training. Then, compared with the raw SA-CDNet, we drop the adaptive fusion module and incorporate an additional semantic segmentation head to the semantic-aware decoder for a proxy single-temporal segmentation task. This pre-training strategy enhances the knowledge about the landscape, beneficial to the change detection task.

difference-aware decoder branch is formulated as,

$$\hat{Y}_c = \mathcal{N}(\{F_i, F'_i\}_{i=2,3,4,5}). \quad (5)$$

In contrast to the semantic-aware decoder that deals with bi-temporal image features individually, this difference-aware decoder mines difference-aware features from rich multi-scale features of bi-temporal images, thus helping to discriminate change regions as validated in Sec. IV-B. It is sensitive to changes of various scales and handles details effectively.

3) **Adaptive fusion module:** As mentioned, the semantic-aware decoder excels at capturing semantic-aware and contextual features, and the multi-scale difference-aware decoder prevails in perceiving fine-grained difference-aware features. We employ a simple adaptive fusion module to incorporate the difference-aware features and semantic-aware features for final results. For simplicity, we introduce a learnable weight $\sigma(\omega)$ to integrate the predictions from the two decoders, where $\sigma(\cdot)$ denotes the sigmoid function. This fusion strategy obtained a better trade-off between the precision and recall as discussed in Tab. V. Thus, the final prediction \hat{Y} is computed as,

$$\hat{Y} = \sigma(\omega) * \hat{Y}_s + (1 - \sigma(\omega)) * \hat{Y}_c. \quad (6)$$

B. Single-temporal Semantic Pre-training Strategy

Though our proposed SA-CDNet utilizes the vision foundation model and a dual-stream feature decoder to enhance the semantic understanding of the landscapes, we suppose it still under-explores the semantic priors for change detection. The reasons are two-fold. First, existing change detection datasets are limited and small in scale, as manually collecting registered bi-temporal images and corresponding changed-region annotation are costly and challenging, let alone high-quality ones. Besides, datasets contain specific interested changes are also scarce. Second, most datasets only provide binary change maps for training, which fails to provide other useful

information. For example, there is no information about the landscape category before and after the changes. The above two facts restrict semantic learning when training on change detection datasets. To solve the issue, we propose a single-temporal semantic pre-training strategy with massive pseudo-change detection data, largely enriching the semantic priors in the network. Here are detailed instructions.

1) **Pseudo-change data construction:** To relieve the data scarcity issue, we adopt the public remote sensing segmentation dataset to construct large-scale bi-temporal images with pseudo-change annotations for pre-training. We choose the segmentation dataset for two reasons: i) Owing to the lower cost of collecting single-temporal images and the segmentation masks, the data scale of remote sensing segmentation datasets is larger than that of change detection as illustrated in Tab. I and Tab. II. ii) The semantic segmentation datasets naturally provide the semantic masks of the interested landscapes of each single-temporal image, offering better supervision for learning semantics. Specifically, we extend the task of detecting changes between registered bi-temporal images to identifying differences of interested landscapes between any two remote sensing images. Given the semantic segmentation dataset $\mathcal{D} = (X_i, Y_i)_{i=1 \sim N}$, we randomly sample two single-temporal image samples (X_i, Y_i) and (X_j, Y_j) . As shown in Fig. 4, we treat the two images as pseudo-bi-temporal images, where $\tilde{X}_k = X_i$ and $\tilde{X}'_k = X_j$. The change label is computed as the XOR of the segmentation maps, where $\tilde{Y}_k = Y_i \oplus Y_j$. Thus, the newly pseudo-change detection dataset $\tilde{\mathcal{D}}$ can be denoted as,

$$\tilde{\mathcal{D}} = \{(\tilde{X}_k, \tilde{X}'_k, \tilde{Y}_k^{seg}, \tilde{Y}'_k^{seg}, \tilde{Y}_k)_{k=1 \sim K} | \tilde{X}_k = X_i, \tilde{X}'_k = X_j, \tilde{Y}_k^{seg} = Y_i, \tilde{Y}'_k^{seg} = Y_j, \tilde{Y}_k = Y_i \oplus Y_j\}, \quad (7)$$

where $(X_i, Y_i), (X_j, Y_j) \in \mathcal{D}$, and K is the number of pseudo-change detection samples. One advantage of the pseudo-change data is that both the change map for bi-temporal images

and the semantic map for each single-temporal image are available. Note that we can construct at most $K = \binom{2}{N} \gg N$ samples from N single-scale semantic segmentation samples, which considerably enlarges the available data for pre-training. This strategy also leads to diverse samples.

2) **Semantic learning pre-training:** Pre-training endows the network with basic knowledge about images from extensive data with proxy training objectives. It is widely used to relieve the data scarcity issue of downstream tasks. For example, researchers would use ImageNet pre-trained parameters to initialize the backbone ResNet or ViT [37, 38]. Thus, we employ the pseudo-change detection dataset \tilde{D} to pre-train SA-CDNet, which provides knowledge about remote sensing images and semantic understandings of the landscape.

As illustrated in Fig. 4, we still freeze FastSAM encoder to keep its knowledge intact and pre-train the rest of modules on the constructed dataset, *i.e.*, the adapter and the dual-stream decoder. While the whole network structure is unchanged, we dropped the adaptive fusion module. Moreover, we introduce an extra semantic segmentation head $\mathcal{S}(\cdot)$ as the semantic-aware decoder branch, which is constructed by one `conv + batch norm + ReLU` block and a `conv + softmax` layer. The segmentation head receives fused single-temporal feature $D_1(D'_1)$ from the semantic-aware decoder branch, and predicts its segmentation map $\hat{Y}_{seg}(\hat{Y}'_{seg})$ individually, which is formulated as,

$$\hat{Y}_{seg} = \mathcal{S}(D_1), \quad \hat{Y}'_{seg} = \mathcal{S}(D'_1), \quad (8)$$

where \hat{Y}_{seg} and \hat{Y}'_{seg} are predicted semantic map for each image. We also impose constraints to \hat{Y}_{seg} and \hat{Y}'_{seg} and treat it as a proxy semantic segmentation task for semantic pre-training, thanks to the available single-temporal segmentation masks in the pseudo-change dataset. This design exploits the semantic maps to enhance the semantic priors of the interested landscapes. The evidence is revealed in Sec. IV-C.

C. The Overall Training Strategy for SA-CDNet

We employ a “pre-training + fine-tuning” pipeline to train SA-CDNet following common practices [39, 40]. In the single-temporal semantic pre-training phase, we train SA-CDNet with the additional semantic segmentation head $\mathcal{S}(\cdot)$ on the pseudo-change dataset \tilde{D} , to distill the knowledge of remote sensing images and landscapes from massive pseudo-bi-temporal images. Then, we fine-tune SA-CDNet on change detection datasets for the final prediction. Here are more details including the loss functions.

1) **Pre-training:** Given the constructed pseudo-change detection dataset \tilde{D} in Sec. III-B1, we freeze the vision foundation model encoder $\mathcal{E}(\cdot)$ and train the change detection adapter $\mathcal{A}(\cdot)$, the semantic-aware decoder branch $\mathcal{M}(\cdot)$ and the multi-scale difference-aware decoder branch $\mathcal{N}(\cdot)$ of the dual-stream feature decoder. Note that the adaptive fusion module is dropped in the pre-training stage. Additionally, a semantic segmentation head is appended to the semantic-aware decoder $\mathcal{S}(\cdot)$ to predict the semantic map of each single-temporal image. Two training objectives are adopted for pre-training, *i.e.*, pseudo-change detection and single-temporal semantic

segmentation. For the pseudo-change detection, we compute the binary cross-entropy loss for the predicted change maps from the two decoder branches, formulated as,

$$L_{CD} = L_{CD}^s + L_{CD}^c = \mathcal{L}_{ce}(\hat{Y}_s, \tilde{Y}) + \mathcal{L}_{ce}(\hat{Y}_c, \tilde{Y}) \quad (9)$$

where L_{CD}^s and L_{CD}^c are the losses of semantic-aware and difference-aware decoder branch, respectively. $\mathcal{L}_{ce}(\cdot)$ is the cross-entropy loss function.

For the proxy single-temporal semantic segmentation task, the loss is computed as,

$$L_{seg} = \mathcal{L}_{ce}(\hat{Y}_{seg}, \tilde{Y}_{seg}) + \mathcal{L}_{ce}(\hat{Y}'_{seg}, \tilde{Y}'_{seg}), \quad (10)$$

where \hat{Y}_{seg} and \hat{Y}'_{seg} are the predicted semantic map of bi-temporal images from the segmentation head. Thus, the total loss of the pre-training phase consists of two parts, which can be expressed as follows:

$$L_{pt} = L_{CD} + \lambda \cdot L_{seg}, \quad (11)$$

where λ is the coefficient to balance the two pre-training objectives. λ is empirically set to 1.0 in our experiments.

2) **Fine-tuning:** While the network learns to predict the changes after the pre-training, this model still performs weakly in the real scenes. Evidence can be found in Tab. VII. This is because the pre-training only equips the network with basic understandings of remote sensing images and semantic priors of landscapes from the large-scale pseudo-change data. But there still exists a large gap (*e.g.*, seasonal and illumination variations) between the pseudo-change data and real ones. Therefore, it is necessary to adapt such knowledge and priors to the real bi-temporal images and interested changes through fine-tuning on the change detection datasets.

Specifically, we initialize SA-CDNet with the single-temporal semantic pre-training parameters and further fine-tune the network on the change detection dataset. The vision foundation model encoder $\mathcal{E}(\cdot)$ is still frozen. Since existing change detection datasets only provide bi-temporal images and corresponding change map, the semantic segmentation head $\mathcal{S}(\cdot)$ is dropped in the fine-tuning phase. We fine-tune the change detection adapter $\mathcal{A}(\cdot)$, the semantic-aware decoder branch $\mathcal{M}(\cdot)$ and the multi-scale difference-aware decoder branch $\mathcal{N}(\cdot)$ of the dual-stream feature decoder, and the adaptive fusion module. The overall loss for the fine-tuning phase only contains the change detection loss from the dual-stream feature decoder and the adaptive fusion module, which is computed as,

$$\begin{aligned} L_{ft} &= L_{CD}^s + L_{CD}^c + L_{CD}^f \\ &= \mathcal{L}_{ce}(\hat{Y}_s, Y) + \mathcal{L}_{ce}(\hat{Y}_c, Y) + \mathcal{L}_{ce}(\hat{Y}, Y), \end{aligned} \quad (12)$$

where \hat{Y}_s and \hat{Y}_c are the predictions of the dual-stream feature decoder. \hat{Y} is the final prediction produced by the adaptive fusion module, which is empirically better than \hat{Y}_s and \hat{Y}_c .

IV. EXPERIMENTS

A. Experimental Setup

1) **Datasets and evaluation metrics:** We conduct experiments on two kinds of datasets: **i) Remote sensing semantic**

TABLE I: Detailed information about the semantic segmentation datasets utilized for pre-training.

Dataset	Spatial Resolution	Image Size	Image Number	Class Number	Class Information
AIRS [41]	0.075 m	10,000×10,000	1,046	1	Building
INRIA-Building [42]	0.3 m	5,000 × 5,000	180	1	Building
WHU-Building [43]	0.3 m	512 × 512	8,189	1	Building
DLCCC [44]	0.5 m	2,448 × 2,448	803	7	Agriculture, barren, forest, rangeland, urban, unknown, water
LoveDA [45]	0.3 m	1,024 × 1,024	5,987	7	Agriculture, barren, building, background, forest, road, water

TABLE II: Detailed information about change detection datasets used for experiments.

Dataset	Spatial Resolution	Image Size	Image Number	Train/Val/Test	Cropped Size	Classes
LEVIR-CD [46]	0.5 m	1,024 × 1,024	637	445 : 64 : 128	256 × 256	Building
LEVIR-CD+ [46]	0.5 m	1,024 × 1,024	985	637 : 0 : 384	256 × 256	Building
S2Looking [47]	0.5~0.8 m	1,024 × 1,024	5,000	3,500 : 500 : 1,000	256 × 256	Building
WHU-CD [43]	0.075 m	32,507 × 15,354	1	–	256 × 256	Building
WHU Cultivated Land [48]	1~2 m	512 × 512	3,194	2,694 : 0 : 500	–	Farmland

segmentation datasets. We utilize three single-class segmentation datasets, (*i.e.*, AIRS [41], INRIA-Building [42], and WHU-Building [43], for buildings) and two multi-class semantic segmentation datasets (*i.e.*, DLCCC [44] and LoveDA [45], for 7-class landscapes within agriculture, roads, water, *etc.*) for pre-training. These datasets are used to construct pseudo-change data during the pre-training phase. **ii) Change detection datasets.** We evaluate our method on four building change datasets (*i.e.*, LEVIR-CD [46], LEVIR-CD+ [46], S2Looking [47], WHU-CD [43]) and one farmland change dataset (*i.e.*, the WHU Cultivated Land dataset [48]). Details about each dataset refer to Tab. I and Tab. II. Following previous works [21, 24, 33], we report the precision, recall, and F1-score as evaluation metrics for all experiments.

2) **Implementation details:** We conduct all experiments with PyTorch on 8× 32GB NVIDIA Tesla V100 GPU. We employ the SGD optimizer with a weight decay of 0.0005 and a momentum of 0.9. The batch size is 32, and the learning rate decayed following an exponential schedule. During pre-training, we crop all images into 512 × 512 without overlap offline and randomly pick samples from the cropped segmentation dataset to generate the pseudo-change data online. We pre-train the model for 200 epochs with an initial learning rate of 0.1. During fine-tuning, we fine-tune the network on the change detection dataset for 50 epochs with an initial learning rate of 0.01. For fair comparison with previous methods, we crop images into unified size as listed in Tab. II. To enhance the robustness of the model, we employ some commonly used data augmentation strategies, such as random flips, random rotation, random added noise, and normalization.

B. Ablation Study

We conduct comprehensive ablation studies mainly from two aspects: **i)** verify the effectiveness of proposed modules, and **ii)** compare and discuss different settings for pre-training to obtain the optimal one.

1) **Ablations for model design:** We first compare the performance of feature encoders from different vision foundation

models, then ablate the change detection adapter and each of the two branches in the dual-stream feature decoder. We also discuss different fusion strategies for the adaptive fusion module. All experiments were conducted on WHU-CD for consistent evaluation. Note that we did not use the proposed pre-training strategy in this section.

Comparison of different vision foundation model encoders. We select SAM and its three variants as the candidates to compare their performance and efficiency for encoding features. We utilize different-sized versions of the foundation model, including SAM-b (*basic*), SAM-l (*large*), SAM-h (*huge*), EfficientSAM-t (*lightweight*), EfficientSAM-s (*standard*), and FastSAM-s (*lightweight*), FastSAM-x (*extended version*). Considering the distinct model structures, we only utilize the encoder of these models to extract bi-temporal image features. Then we feed these features to a change detection module consisting of one conv + sigmoid layer and trained it on WHU-CD to produce the change map. The results are listed in Tab. III, where the SAM-h was excluded due to the computation limitation.

As shown in Tab. III, while the SAM-series encoders achieved the best F1-score, *i.e.*, SAM-b of 77.17% and SAM-l of 81.81%, they also had the largest model size and computation costs. These results reflected that SAM could provide powerful feature representations, but its heavy computation costs somehow limited its application to downstream tasks. In contrast, FastSAM-series encoders exhibit the best FLOPs with the third-highest F1-score as 74.60%, which is far more efficient than SAM with acceptable performance. Therefore, we choose FastSAM-x as our feature encoder in all experiments for a trade-off between performance and efficiency.

Effects of each modules. We study the effectiveness of the proposed change detection adapter $\mathcal{A}(\cdot)$, the semantic-aware decoder branch $\mathcal{M}(\cdot)$ and multi-scale difference-aware decoder branch $\mathcal{N}(\cdot)$. The results are reported in Tab. IV.

All modules contribute to the final performance and complement each other. The change detection adapter $\mathcal{A}(\cdot)$ improve the precision and recall by a large margin of 23.86% and 4.11%, resulting in an improvement of 13.52% F1-score. This

TABLE III: Comparison of performance and efficiency of different vision foundation model encoders, where **bold** for the optimal result and underline for the second-best one.

Model	Computation Complexity		Metric		
	Params(Mb)	FLOPs(G)	P(%)	R(%)	F1(%)
MobileSAM	6.33	75.93	42.41	71.38	53.22
EfficientSAM-t	<u>6.72</u>	52.52	75.65	70.18	72.81
EfficientSAM-s	22.87	184.74	76.84	70.74	73.66
FastSAM-s	11.22	1.85	75.21	63.19	68.68
FastSAM-x	68.23	<u>6.32</u>	71.91	<u>77.49</u>	74.60
SAM-b	87.03	740.45	92.47	66.21	<u>77.17</u>
SAM-l	304.54	2626.37	<u>85.93</u>	78.06	81.81
SAM-h	632.18	5470.24	—	—	—

TABLE IV: The effects of each module. $\mathcal{A}(\cdot)$ denotes the adapter, $\mathcal{M}(\cdot)$ denotes the semantic-aware decoder, and $\mathcal{N}(\cdot)$ denotes the multi-scale difference-aware decoder.

Module			Metric		
$\mathcal{A}(\cdot)$	$\mathcal{M}(\cdot)$	$\mathcal{N}(\cdot)$	P(%)	R(%)	F1(%)
			71.91	77.49	74.60
✓			95.77	81.60	88.12
✓	✓		93.60	88.55	91.00
✓		✓	94.33	89.86	92.04
✓	✓	✓	94.66	91.22	92.91

fact confirms the gap between natural images and remote sensing images, exhibiting the necessity of the adapter. As for the dual-stream feature decoder, when the multi-scale difference-aware decoder bring an increment of 3.92% F1-score, our semantic-aware decoder further improve it by 0.87%. The results show that the multi-scale difference features are vital to change detection, and incorporating semantic understandings into the network brings further advantages. Our method achieve the optimal performance by combining all modules with a 92.91% F1-score, surpassing the baseline by 18.31%.

Comparison of different strategies for adaptive fusion module. Inspired by the ensemble learning, we explore to combine predictions from the two decoder branches with varied strategies. We test three strategies, including computing the max and mean value, and using a learnable weight $\sigma(\omega)$. As listed in Tab. V, max fusion benefited the recall, while mean fusion benefited the precision. Fusion with a learnable weight obtained a trade-off with the best 92.91% F1-score.

2) **Ablations for pre-training strategy:** We first validate the effectiveness of the semantic segmentation head, then explore different settings and combinations of the remote sensing semantic segmentation datasets and analyze their impacts on pre-training. Here we train the network on the pseudo-change dataset and reported its performance on WHU-CD for consistent comparison. We suppose that higher performance on the unseen WHU-CD dataset indicates better knowledge on remote sensing images after the pre-training.

Effects of the semantic segmentation head $\mathcal{S}(\cdot)$. We ablate the semantic segmentation head on three buildings change detection datasets as presented in Tab. VI. Equipped with the proposed segmentation head $\mathcal{S}(\cdot)$, the performance increased consistently on all datasets, where the F1-score increased

TABLE V: Comparison of different fusion strategies.

Fusion Strategy	P(%)	R(%)	F1(%)
Max	93.08	91.82	92.44
Mean	95.27	90.01	92.57
Learnable weight	94.66	91.22	92.91

TABLE VI: The effects of the semantic segmentation head on the pre-trained phase.

Dataset	Experiment Setting	Metric		
	$\mathcal{S}(\cdot)$	P(%)	R(%)	F1(%)
AIRS	×	48.75	92.18	63.77
	✓	50.88	92.94	65.76
INRIA-Building	×	47.06	86.83	61.04
	✓	46.84	93.35	62.38
WHU-Building	×	57.82	91.75	70.93
	✓	58.82	93.21	72.12

1.99% on AIRS, 1.34% on INRIA-Building, and 1.09% on WHU-Building. This indicates that the segmentation head $\mathcal{S}(\cdot)$ encourages models to learn semantic priors of the landscapes.

Comparison of single-class and multi-class segmentation datasets for pre-training. We employ two kinds of remote sensing semantic segmentation datasets for pre-training: **i)** three single-class segmentation datasets for buildings (*i.e.*, AIRS, INRIA-Building, and WHU-Building), and **ii)** two multi-class semantic datasets (*i.e.*, DLCCC and LoveDA) for buildings, roads, water, *etc.* Since the downstream change detection dataset (*i.e.*, WHU-CD) only concerns building changes, we discuss the effects of different kinds of datasets on the pre-training. We train the network on each dataset and compared their performance in Tab. VII. For fairness, we kept the same number of training samples for all experiments.

As illustrated in Tab. VII, the model trained on WHU-Building achieved the best performance due to the smallest appearance gap to WHU-CD. Moreover, the models trained on the buildings' single-class semantic segmentation datasets outperformed those trained on the multi-class semantic segmentation datasets by a large margin. We suppose that the models trained on the multi-class semantic segmentation datasets were confused by different landscape types, resulting in comparable recall but much lower precision than those trained on the single-class segmentation datasets.

To validate this assumption and avoid the potential bias caused by images, we filter irrelevant categories and only keep the semantic annotations according to the downstream task. Specifically, we take farmland changes for experiments and construct alternative datasets by removing the other semantic annotations, namely DLCCC-Cultivation and LoveDA-Cultivation. This setting ensure that only the number of annotated categories was different between the two datasets. We use the above datasets for training and report the performance on WHU Cultivated Land in Tab. VIII. Both models trained with single-class annotations outperform those trained with multi-class annotations, with an obvious increment of about 10% F1-score under both settings. Therefore, it is better to employ the segmentation datasets with the same category as the downstream change detection task for pre-training.

TABLE VII: Effects of single-class and multi-class segmentation datasets on the pre-training.

Dataset	P(%)	R(%)	F1(%)
AIRS	50.88	92.94	65.76
INRIA-Building	46.84	93.35	62.38
WHU-Building	58.82	93.21	72.12
DLCCC	24.69	89.61	38.71
LoveDA	28.12	89.40	42.78

TABLE VIII: Comparison of single-class and multi-class semantic segmentation annotations for the pre-training.

Dataset	P(%)	R(%)	F1(%)
DLCCC	70.66	28.97	41.09
DLCCC-Cultivation	65.10	42.46	51.50
LoveDA	65.22	30.76	41.80
LoveDA-Cultivation	65.07	44.22	52.66

Including annotations of other landscape categories would disturb the representations of interested changes.

Effects of different combinations of segmentation datasets for pre-training. Considering remote sensing images from the same dataset were captured during close time periods on the neighboring regions, they would share similar data distribution. This potentially limited the diversity of the pseudo-change data. To this end, we combine different datasets for pre-training to explore the effects of data diversity. For fairness, we employ the same number of training samples among different combinations in this section. If there were multiple datasets, the proportion for them would be 1:1. Tab. X presents the results on WHU-CD and WHU-Cultivated Land. We notice that the more diverse datasets used for pre-training, the higher performance they would achieve. This observation is consistent among all experiments. Thus, the combination of all single-class segmentation datasets of the same category for pre-training yielded the best performance. We use all building segmentation datasets (*i.e.*, AIRS, INRIA-Building, and WHU-Building) to pre-train the model for building change detection and the filtered datasets with only the farmland (*i.e.*, DLCCC-Cultivation and LoveDA-Cultivation) for farmland changes.

C. Comparison with Fully Supervised Methods

To demonstrate the superiority of our SA-CDNet, we conduct experiments on several challenging datasets, including four building change datasets (*i.e.*, LEVIR-CD, LEVIR-CD+, S2Looking, WHU-CD) and one cultivation change dataset (*i.e.*, WHU Cultivated Land). The comparison results are reported in Tab. IX, where both of our method with and without the pre-training are listed for comprehensive comparisons.

As shown in Tab. IX, our method achieve the best F1-score on all five datasets, outperforming the current SOTA methods even without the proposed single-temporal semantic pre-training. Specifically, our method without pre-pretraining surpass the current SOTA method by 0.14% F1-score on LEVIR-CD, 0.66% on LEVIR-CD+, 1.98% on S2Looking, 0.7% on WHU-CD, and 1.0% on WHU Cultivated Land. Equipped with the proposed pre-training strategy with the

pseudo-change data, our method obtain the best performance, setting new SOTA on five datasets with a 91.53% F1-score on LEVIR-CD, a 84.43% F1-score on LEVIR-CD+, a 66.48% F1-score on S2Looking, a 94.47% F1-score on WHU-CD, and a 75.20% F1-score on LEVIR-CD+, which also surpass the results without pre-training by a large margin. Moreover, our method exhibit more significant increments on more challenging datasets like LEVIR-CD+, S2Looking, and WHU Cultivated Land, which contains complex background and delicate changes. These results prove the advance of SA-CDNet and the single-temporal semantic pre-training strategy, demonstrating the significance of the semantic priors of the landscapes in change detection tasks.

The visualized comparisons are presented in Fig. 5. For page limitations, we only show the results of recent advanced methods. As shown in Fig. 5, our method excels at capturing fine details along boundaries and subtle changes. For example, our method keeps more clear boundaries of the changed regions compared to other methods as illustrated in the 1st, 3rd, 4th, 5th, 7th, 8th rows of samples. We attribute these benefits to better semantic understandings of the landscapes, producing more complete and clear regions. This fact proves the effectiveness of SA-CDNet and the semantic pre-training strategy. Incorporating semantics into change detection also helps to avoid false positive and false negative predictions as shown in the 2nd, 6th, 7th rows of samples. Moreover, when facing challenging farmland changes with arbitrary shapes in the WHU Cultivated Land, SA-CDNet can produce faithful and robust results with precise boundaries. This fact further verifies the capability of our method of detecting other challenging categories of changes besides the building.

D. Comparison with Semi-supervised Methods

SA-CDNet with the pre-training strategy also provides a solution when only limited annotated change detection data is available. We validate this by comparing SA-CDNet with three recent semi-supervised change detection methods, including SemiCDNet [54], SemiSANet [55], and MTCNet [56] under the semi-supervised learning setup. To reduce the cost of human annotations, the semi-supervised methods aim to learn from large-scale unlabeled data with the help of limited labeled data. Popular semi-supervised learning techniques utilize consistency regularization and pseudo-labels to mine useful information from large-scale unlabeled data. Here, we test the three semi-supervised methods on WHU-CD under the settings of 5%, 10%, 20%, and 40% labels. All bi-temporal images are accessible during the training if needed. Our method only use the labeled images for training and ignore the unlabeled ones.

The comparison results are listed in Tab. XI. Our method without pre-training achieved comparable results with the optimal method MTCNet under the 5% and 10% settings. As the number of available labels grew, our method without pre-training outperformed the semi-supervised methods. Even with limited labeled data, SA-CDNet can exhibit promising results, reflecting the data efficiency of our method. Moreover, taking advantage of the prior knowledge learned from the single-temporal semantic pre-training, our method with pre-training

TABLE IX: Comparisons of our method with existing SOTA methods on the LEVIR-CD, LEVIR-CD+, S2Looking, WHU-CD, and WHU Cultivated Land dataset.

Method	LEVIR-CD			LEVIR-CD+			S2Looking			WHU-CD			WHU Cultivated Land		
	P(%)	R(%)	F1(%)	P(%)	R(%)	F1(%)	P(%)	R(%)	F1(%)	P(%)	R(%)	F1(%)	P(%)	R(%)	F1(%)
FC-EF [20]	86.91	80.17	83.40	76.49	76.32	76.41	<u>81.36</u>	8.95	7.65	80.75	67.29	73.40	60.29	62.98	61.61
FC-Siam-conc [20]	91.99	76.77	83.69	81.12	77.16	79.09	68.27	18.52	13.54	54.20	81.34	65.05	62.51	65.24	63.85
FC-Siam-diff [20]	89.53	83.31	86.31	80.88	77.65	79.23	83.49	32.32	46.60	48.84	88.96	63.06	64.81	56.42	60.33
STANet [49]	83.81	<u>91.00</u>	87.26	74.20	83.90	78.80	36.40	<u>68.20</u>	47.40	77.40	90.30	83.35	62.75	69.47	65.94
DASNet [50]	80.76	79.53	79.91	77.51	78.03	77.77	45.06	48.71	47.29	83.77	91.02	87.24	60.58	77.00	67.81
SNUNet [21]	89.18	87.17	88.16	78.90	78.23	78.56	45.25	50.60	47.78	91.28	87.25	89.22	68.88	72.09	70.45
BIT [24]	92.57	87.65	90.04	82.37	79.73	81.03	70.26	56.53	62.65	91.56	87.84	89.66	70.84	70.11	70.48
FTN [51]	92.71	89.37	91.01	80.91	<u>83.47</u>	82.17	61.54	60.26	63.19	94.73	89.83	92.21	<u>75.54</u>	63.20	68.82
VcT [52]	89.24	89.37	89.31	80.50	81.41	80.95	61.49	68.25	62.30	93.24	76.58	84.09	65.90	66.74	66.32
RFL-CDNet [53]	91.62	90.40	90.98	79.95	84.04	81.94	65.72	60.82	63.17	91.33	<u>91.46</u>	91.39	70.87	73.75	72.28
SAM-CD [33]	91.38	90.45	90.91	79.71	81.35	81.96	74.32	55.30	63.42	96.87	85.67	90.92	68.80	73.12	70.89
Ours (<i>w/o pre-train</i>)	<u>92.69</u>	89.66	<u>91.15</u>	86.88	79.15	<u>82.83</u>	81.25	54.73	<u>65.40</u>	94.66	91.22	<u>92.91</u>	72.65	<u>73.93</u>	<u>73.28</u>
Ours (<i>w pre-train</i>)	91.77	91.28	91.53	<u>85.55</u>	83.44	84.43	81.28	56.24	66.48	<u>95.29</u>	93.67	94.47	77.74	72.82	75.20

TABLE X: Effects of different dataset combinations for pre-training.

Dataset			Metric		
AIRS	INRIA-Building	WHU-Building	P(%)	R(%)	F1(%)
✓			50.88	92.94	65.76
	✓		46.84	93.35	62.38
		✓	58.82	93.21	72.12
✓	✓		53.74	94.16	68.42
✓		✓	64.57	91.30	75.64
	✓	✓	62.10	93.72	73.70
✓	✓	✓	65.48	92.41	76.65
DLCCC-Cultivation		LoveDA-Cultivation	P(%)	R(%)	F1(%)
	✓		65.10	42.46	51.50
		✓	65.07	44.22	52.66
	✓	✓	59.87	51.00	55.08

TABLE XI: Comparison results on WHU-CD under the semi-supervised setup.

Method	Proportion of labeled data			
	5%	10%	20%	40%
SemiCDNet [54]	82.90	85.28	86.57	87.74
SemiSAnet [55]	80.95	85.32	86.99	88.36
MTCNet [56]	<u>87.63</u>	<u>89.63</u>	90.64	91.46
Ours (<i>w/o pre-train</i>)	87.33	89.57	<u>91.18</u>	<u>92.17</u>
Ours (<i>w/ pre-train</i>)	89.63	92.77	93.77	94.13

perform best under all settings. These results demonstrate the advance of our pre-training strategy in reducing the reliance on large-scale annotated data for training. It also relieves potential problems like over-fitting and under-fitting when only limited training data are available.

E. Model Size and Computational Complexity

Tab. XII presents the model size and computational complexity of our method and some previous SOTA methods. Though our method contains the highest 77.08MB parameters, we highlight most parameters are frozen, where the frozen FastSAM encoder contains 68MB parameters, and only 9.08MB parameters are trained. The FLOPs of our methods

TABLE XII: Model size and computational complexity.

Method	Params(Mb)	Trainable Params(Mb)	FLOPs(G)
STANet [49]	<u>16.93</u>	16.93	6.58
DASNet [50]	48.22	48.22	25.17
SNUNet [21]	27.07	27.07	27.44
BIT [24]	11.47	11.47	19, 60
RFL-CDNet [53]	27.24	27.24	33.89
SAM-CD [33]	70.49	2.49	<u>8.60</u>
Ours	77.08	<u>9.08</u>	12.03

is 12.03G, a little higher than that of STANet (6.58G) and SAM-CD (8.60G), but significantly lower than other recent advanced methods. However, since our method achieves SOTA performance on several change detection benchmarks and surpasses the second-highest one by a large margin, we think that a little increment of FLOPs is acceptable.

V. CONCLUSION

To achieve advanced change detection performance, we argue that the network requires to not only perceive the difference between the bi-temporal images but also have knowledge of the remote sensing landscapes. To this end, this paper proposes a novel SA-CDNet with a single-temporal semantic pre-training strategy to incorporate semantic priors into change detection. Our SA-CDNet mainly consists of a vision foundation model-based feature encoder to inherit its knowledge of natural images, an adapter to align features with change detection, and a dual-stream feature decoder to exploit difference-aware features and semantic-aware features for change detection, which follows the human visual paradigm to distinguish changes. With the help of semantic pre-training, SA-CDNet learns richer semantic priors about the interested landscapes in the remote sensing context from the pseudo-change data. We conducted comprehensive experiments on several challenging change detection datasets, where our method achieved the SOTA performance. Detailed ablation studies validated the effectiveness of our designs of both the network structure and the semantic pre-training strategy.

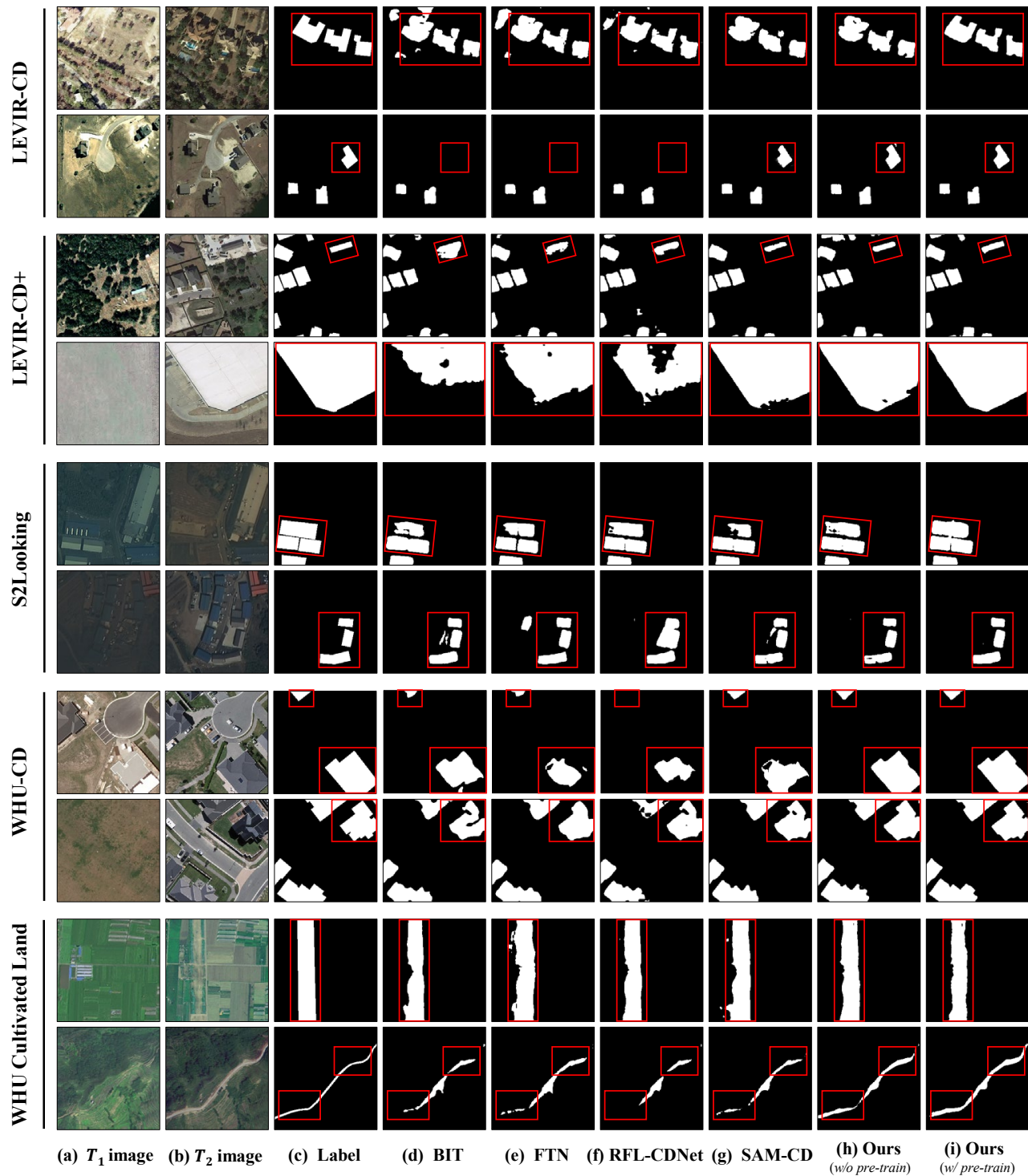


Fig. 5: Visualized comparison of our method with previous SOTA methods.

REFERENCES

- [1] Z. Lv, H. Huang, X. Li, M. Zhao, J. A. Benediktsson, W. Sun, and N. Falco, "Land cover change detection with heterogeneous remote sensing images: Review, progress, and perspective," *Proceedings of the IEEE*, vol. 110, no. 12, pp. 1976–1991, 2022.
- [2] D. Wen, X. Huang, F. Bovolo, J. Li, X. Ke, A. Zhang, and J. A. Benediktsson, "Change detection from very-high-spatial-resolution optical remote sensing images: Methods, applications, and future directions," *IEEE Geoscience and Remote Sensing Magazine*, vol. 9, no. 4, pp. 68–101, 2021.
- [3] C. Wu, L. Zhang, B. Du, H. Chen, J. Wang, and H. Zhong, "Unet-like remote sensing change detection: A review of current models and research directions," *IEEE Geoscience and Remote Sensing Magazine*, 2024.
- [4] D. Peng, Y. Zhang, and H. Guan, "End-to-end change detection for high resolution satellite images using improved unet++," *Remote Sensing*, vol. 11, no. 11, p. 1382, 2019.
- [5] C. Zhang, P. Yue, D. Tapete, L. Jiang, B. Shangguan,

- L. Huang, and G. Liu, "A deeply supervised image fusion network for change detection in high resolution bi-temporal remote sensing images," *ISPRS Journal of Photogrammetry and Remote Sensing*, vol. 166, pp. 183–200, 2020.
- [6] W. G. C. Bandara and V. M. Patel, "A transformer-based siamese network for change detection," in *IGARSS 2022-2022 IEEE International Geoscience and Remote Sensing Symposium*, 2022, pp. 207–210.
- [7] W. Liu, Y. Lin, W. Liu, Y. Yu, and J. Li, "An attention-based multiscale transformer network for remote sensing image change detection," *ISPRS Journal of Photogrammetry and Remote Sensing*, vol. 202, pp. 599–609, 2023.
- [8] H. Chen, W. Li, S. Chen, and Z. Shi, "Semantic-aware dense representation learning for remote sensing image change detection," *IEEE Transactions on Geoscience and Remote Sensing*, vol. 60, pp. 1–18, 2022.
- [9] X. Zhang, X. Huang, and J. Li, "Semisupervised change detection with feature-prediction alignment," *IEEE Transactions on Geoscience and Remote Sensing*, vol. 61, pp. 1–16, 2023.
- [10] D. Wang, L. Jiao, J. Chen, S. Yang, and F. Liu, "Changes-aware transformer: Learning generalized changes representation," *arXiv preprint arXiv:2309.13619*, 2023.
- [11] J. Liu, W. Xuan, Y. Gan, Y. Zhan, J. Liu, and B. Du, "An end-to-end supervised domain adaptation framework for cross-domain change detection," *Pattern Recognition*, vol. 132, p. 108960, 2022.
- [12] Y. Tu, T. Yao, L. Li, J. Lou, S. Gao, Z. Yu, and C. Yan, "Semantic relation-aware difference representation learning for change captioning," in *Findings of the association for computational linguistics: ACL-IJCNLP 2021*, 2021, pp. 63–73.
- [13] X. Zhao, W. Ding, Y. An, Y. Du, T. Yu, M. Li, M. Tang, and J. Wang, "Fast segment anything," *arXiv preprint arXiv:2306.12156*, 2023.
- [14] F. Bovolo and L. Bruzzone, "A theoretical framework for unsupervised change detection based on change vector analysis in the polar domain," *IEEE Transactions on Geoscience and Remote Sensing*, vol. 45, no. 1, pp. 218–236, 2006.
- [15] A. A. Nielsen, "The regularized iteratively reweighted mad method for change detection in multi-and hyper-spectral data," *IEEE Transactions on Image processing*, vol. 16, no. 2, pp. 463–478, 2007.
- [16] J. Im and J. R. Jensen, "A change detection model based on neighborhood correlation image analysis and decision tree classification," *Remote Sensing of Environment*, vol. 99, no. 3, pp. 326–340, 2005.
- [17] S. E. Sesnie, P. E. Gessler, B. Finegan, and S. Thessler, "Integrating landsat tm and srtm-dem derived variables with decision trees for habitat classification and change detection in complex neotropical environments," *Remote Sensing of Environment*, vol. 112, no. 5, pp. 2145–2159, 2008.
- [18] H. Nemmour and Y. Chibani, "Multiple support vector machines for land cover change detection: An application for mapping urban extensions," *ISPRS Journal of Photogrammetry and Remote Sensing*, vol. 61, no. 2, pp. 125–133, 2006.
- [19] M. Hussain, D. Chen, A. Cheng, H. Wei, and D. Stanley, "Change detection from remotely sensed images: From pixel-based to object-based approaches," *ISPRS Journal of photogrammetry and remote sensing*, vol. 80, pp. 91–106, 2013.
- [20] R. C. Daudt, B. Le Saux, and A. Boulch, "Fully convolutional siamese networks for change detection," in *2018 25th IEEE international conference on image processing. IEEE*, 2018, pp. 4063–4067.
- [21] S. Fang, K. Li, J. Shao, and Z. Li, "Snunet-cd: A densely connected siamese network for change detection of vhr images," *IEEE Geoscience and Remote Sensing Letters*, vol. 19, pp. 1–5, 2021.
- [22] A. Dosovitskiy, L. Beyer, A. Kolesnikov *et al.*, "An image is worth 16x16 words: Transformers for image recognition at scale," in *International Conference on Learning Representations*, 2021.
- [23] C. Zhang, L. Wang, S. Cheng, and Y. Li, "Swinsunet: Pure transformer network for remote sensing image change detection," *IEEE Transactions on Geoscience and Remote Sensing*, vol. 60, pp. 1–13, 2022.
- [24] H. Chen, Z. Qi, and Z. Shi, "Remote sensing image change detection with transformers," *IEEE Transactions on Geoscience and Remote Sensing*, vol. 60, pp. 1–14, 2021.
- [25] R. Bommasani, Hudson *et al.*, "On the opportunities and risks of foundation models," *arXiv preprint arXiv:2108.07258*, 2021.
- [26] A. Kirillov, E. Mintun, N. Ravi, H. Mao, C. Rolland, L. Gustafson, T. Xiao, S. Whitehead, A. C. Berg, W.-Y. Lo *et al.*, "Segment anything," in *Proceedings of the IEEE/CVF International Conference on Computer Vision*, 2023, pp. 4015–4026.
- [27] X. Zou, J. Yang, H. Zhang, F. Li, L. Li, J. Wang, L. Wang, J. Gao, and Y. J. Lee, "Segment everything everywhere all at once," in *Advances in Neural Information Processing Systems*, vol. 36, 2023, pp. 19 769–19 782.
- [28] Y. Xiong, B. Varadarajan, L. Wu, X. Xiang, F. Xiao, C. Zhu, X. Dai, D. Wang, F. Sun, F. Iandola *et al.*, "Efficientsam: Leveraged masked image pretraining for efficient segment anything," in *Proceedings of the IEEE/CVF Conference on Computer Vision and Pattern Recognition*, 2024, pp. 16 111–16 121.
- [29] C. Zhang, D. Han, Y. Qiao, J. U. Kim, S.-H. Bae, S. Lee, and C. S. Hong, "Faster segment anything: Towards lightweight sam for mobile applications," *arXiv preprint arXiv:2306.14289*, 2023.
- [30] J. Zhu, Y. Qi, and J. Wu, "Medical sam 2: Segment medical images as video via segment anything model 2," *arXiv preprint arXiv:2408.00874*, 2024.
- [31] J. Ma, Y. He, F. Li, L. Han, C. You, and B. Wang, "Segment anything in medical images," *Nature Communications*, vol. 15, no. 1, p. 654, 2024.
- [32] K. Li, X. Cao, and D. Meng, "A new learning paradigm for foundation model-based remote-sensing change detection," *IEEE Transactions on Geoscience and Remote*

- Sensing*, vol. 62, pp. 1–12, 2024.
- [33] L. Ding, K. Zhu, D. Peng, H. Tang, K. Yang, and L. Bruzzone, “Adapting segment anything model for change detection in vhr remote sensing images,” *IEEE Transactions on Geoscience and Remote Sensing*, 2024.
- [34] L. Mei, Z. Ye, C. Xu, H. Wang, Y. Wang, C. Lei, W. Yang, and Y. Li, “Scd-sam: Adapting segment anything model for semantic change detection in remote sensing imagery,” *IEEE Transactions on Geoscience and Remote Sensing*, 2024.
- [35] T.-Y. Lin, P. Dollar, R. Girshick, K. He, B. Hariharan, and S. Belongie, “Feature pyramid networks for object detection,” in *Proceedings of the IEEE Conference on Computer Vision and Pattern Recognition*, July 2017.
- [36] Q. Wang, B. Wu, P. Zhu, P. Li, W. Zuo, and Q. Hu, “Eca-net: Efficient channel attention for deep convolutional neural networks,” in *Proceedings of the IEEE/CVF conference on computer vision and pattern recognition*, 2020, pp. 11 534–11 542.
- [37] N. Carion, F. Massa, G. Synnaeve, N. Usunier, A. Kirillov, and S. Zagoruyko, “End-to-end object detection with transformers,” in *European conference on computer vision*. Springer, 2020, pp. 213–229.
- [38] Z. Liu, Y. Lin, Y. Cao, H. Hu, Y. Wei, Z. Zhang, S. Lin, and B. Guo, “Swin transformer: Hierarchical vision transformer using shifted windows,” in *Proceedings of the IEEE/CVF international conference on computer vision*, 2021, pp. 10 012–10 022.
- [39] J. Wang, Y. Zhong, and L. Zhang, “Change detection based on supervised contrastive learning for high-resolution remote sensing imagery,” *IEEE Transactions on Geoscience and Remote Sensing*, vol. 61, pp. 1–16, 2023.
- [40] Y. Quan, A. Yu, W. Guo, X. Lu, B. Jiang, S. Zheng, and P. He, “Unified building change detection pre-training method with masked semantic annotations,” *International Journal of Applied Earth Observation and Geoinformation*, vol. 120, p. 103346, 2023.
- [41] Q. Chen, L. Wang, Y. Wu, G. Wu, Z. Guo, and S. L. Waslander, “Temporary removal: Aerial imagery for roof segmentation: A large-scale dataset towards automatic mapping of buildings,” *ISPRS journal of photogrammetry and remote sensing*, vol. 147, pp. 42–55, 2019.
- [42] E. Maggiori, Y. Tarabalka, G. Charpiat, and P. Alliez, “Can semantic labeling methods generalize to any city? the inria aerial image labeling benchmark,” in *2017 IEEE International geoscience and remote sensing symposium*. IEEE, 2017, pp. 3226–3229.
- [43] S. Ji, S. Wei, and M. Lu, “Fully convolutional networks for multisource building extraction from an open aerial and satellite imagery data set,” *IEEE Transactions on geoscience and remote sensing*, vol. 57, no. 1, pp. 574–586, 2018.
- [44] I. Demir, K. Koperski, D. Lindenbaum, G. Pang, J. Huang, S. Basu, F. Hughes, D. Tuia, and R. Raskar, “Deepglobe 2018: A challenge to parse the earth through satellite images,” in *Proceedings of the IEEE conference on computer vision and pattern recognition workshops*, 2018, pp. 172–181.
- [45] A. Song and Y. Kim, “Semantic segmentation of remote-sensing imagery using heterogeneous big data: International society for photogrammetry and remote sensing potsdam and cityscape datasets,” *ISPRS International Journal of Geo-Information*, vol. 9, no. 10, p. 601, 2020.
- [46] H. Chen and Z. Shi, “A spatial-temporal attention-based method and a new dataset for remote sensing image change detection,” *Remote Sensing*, vol. 12, no. 10, p. 1662, 2020.
- [47] L. Shen, Y. Lu, H. Chen, H. Wei, D. Xie, J. Yue, R. Chen, S. Lv, and B. Jiang, “S2looking: A satellite side-looking dataset for building change detection,” *Remote Sensing*, vol. 13, no. 24, p. 5094, 2021.
- [48] “Whu cultivated land dataset,” http://rsipac.whu.edu.cn/subject_two_2021.
- [49] E. Su, S. Cai, L. Xie, H. Li, and T. Schultz, “Stanet: A spatiotemporal attention network for decoding auditory spatial attention from eeg,” *IEEE Transactions on Biomedical Engineering*, vol. 69, no. 7, pp. 2233–2242, 2022.
- [50] J. Chen, Z. Yuan, J. Peng, L. Chen, H. Huang, J. Zhu, Y. Liu, and H. Li, “Dasnet: Dual attentive fully convolutional siamese networks for change detection in high-resolution satellite images,” *IEEE Journal of Selected Topics in Applied Earth Observations and Remote Sensing*, vol. 14, pp. 1194–1206, 2020.
- [51] T. Yan, Z. Wan, and P. Zhang, “Fully transformer network for change detection of remote sensing images,” in *Proceedings of the Asian Conference on Computer Vision*, 2022, pp. 1691–1708.
- [52] B. Jiang, Z. Wang, X. Wang, Z. Zhang, L. Chen, X. Wang, and B. Luo, “Vct: Visual change transformer for remote sensing image change detection,” *IEEE Transactions on Geoscience and Remote Sensing*, 2023.
- [53] Y. Gan, W. Xuan, H. Chen, J. Liu, and B. Du, “Rfl-cdnet: Towards accurate change detection via richer feature learning,” *Pattern Recognition*, vol. 153, p. 110515, 2024.
- [54] D. Peng, L. Bruzzone, Y. Zhang, H. Guan, H. Ding, and X. Huang, “Semidnet: A semisupervised convolutional neural network for change detection in high resolution remote-sensing images,” *IEEE Transactions on Geoscience and Remote Sensing*, vol. 59, no. 7, pp. 5891–5906, 2020.
- [55] C. Sun, J. Wu, H. Chen, and C. Du, “Semisanet: A semi-supervised high-resolution remote sensing image change detection model using siamese networks with graph attention,” *Remote Sensing*, vol. 14, no. 12, p. 2801, 2022.
- [56] Q. Shu, J. Pan, Z. Zhang, and M. Wang, “Mtcnet: Multitask consistency network with single temporal supervision for semi-supervised building change detection,” *International Journal of Applied Earth Observation and Geoinformation*, vol. 115, p. 103110, 2022.